Research Article | Vol. 25, No. 19 | 18 Sep 2017 | OPTICS EXPRESS 22519

Optics EXPRESS

Peak-power scaling of femtosecond Yb:Lu_2O_3 thin-disk lasers

I. J. GRAUMANN,[1,*] A. DIEBOLD,[1] C. G. E. ALFIERI,[1] F. EMAURY,[1] B. DEPPE,[2,3] M. GOLLING,[1] D. BAUER,[4] D. SUTTER,[4] C. KRÄNKEL,[2,5] C. J. SARACENO,[1] C. R. PHILLIPS,[1] AND U. KELLER[1]

[1]*Ultrafast Laser Physics, Institute for Quantum Electronics, ETH Zurich, 8093 Zurich, Switzerland*
[2]*Institut für Laser-Physik, Universität Hamburg, Luruper Chaussee 149, 22761 Hamburg, Germany*
[3]*The Hamburg Center for Ultrafast Imaging, Universität Hamburg, Luruper Chaussee 149, 22761 Hamburg, Germany*
[4]*TRUMPF Laser GmbH, 78713 Schramberg, Germany*
[5]*Center for Laser Materials, Leibniz Institute for Crystal Growth, Max-Born-Str. 2, 12489 Berlin, Germany*
**ivangr@phys.ethz.ch*

Abstract: We present a high-peak-power SESAM-modelocked thin-disk laser (TDL) based on the gain material Yb-doped lutetia (Yb:Lu_2O_3), which exceeds a peak-power of 10 MW for the first time. We generate pulses as short as 534 fs with an average power of 90 W and a peak power of 10.1 MW, and in addition a peak power as high as 12.3 MW with 616-fs pulses and 82-W average power. The center lasing wavelength is 1033 nm and the pulse repetition rates are around 10 MHz. We discuss and explain the current limitations with numerical models, which show that the current peak power is limited in soliton modelocking by the interplay of the gain bandwidth and the induced absorption in the SESAM with subsequent thermal lensing effects. We use our numerical model which is validated by the current experimental results to discuss a possible road map to scale the peak power into the 100-MW regime and at the same time reduce the pulse duration further to sub-200 fs. We consider Yb:Lu_2O_3 as currently the most promising gain material for the combination of high peak power and short pulse duration in the thin-disk-laser geometry.

OCIS codes: (140.3615) Lasers, ytterbium; (140.4050) Mode-locked lasers; (320.7090) Ultrafast lasers.

References and links

1. U. Keller, "Recent developments in compact ultrafast lasers," Nature **424**(6950), 831–838 (2003).
2. K. Sugioka and Y. Cheng, "Ultrafast lasers - reliable tools for advanced materials processing," Light Sci. Appl. **3**(4), e149 (2014).
3. W. Sibbett, A. A. Lagatsky, and C. T. A. Brown, "The development and application of femtosecond laser systems," Opt. Express **20**(7), 6989–7001 (2012).
4. T. Südmeyer, S. V. Marchese, S. Hashimoto, C. R. E. Baer, G. Gingras, B. Witzel, and U. Keller, "Femtosecond laser oscillators for high-field science," Nat. Photonics **2**(10), 599–604 (2008).
5. J.-P. Negel, A. Loescher, A. Voss, D. Bauer, D. Sutter, A. Killi, M. A. Ahmed, and T. Graf, "Ultrafast thin-disk multipass laser amplifier delivering 1.4 kW (4.7 mJ, 1030 nm) average power converted to 820 W at 515 nm and 234 W at 343 nm," Opt. Express **23**(16), 21064–21077 (2015).
6. M. Müller, M. Kienel, A. Klenke, T. Gottschall, E. Shestaev, M. Plötner, J. Limpert, and A. Tünnermann, "1 kW 1 mJ eight-channel ultrafast fiber laser," Opt. Lett. **41**(15), 3439–3442 (2016).
7. P. Russbueldt, T. Mans, J. Weitenberg, H. D. Hoffmann, and R. Poprawe, "Compact diode-pumped 1.1 kW Yb:YAG Innoslab femtosecond amplifier," Opt. Lett. **35**(24), 4169–4171 (2010).
8. J. Aus der Au, G. J. Spühler, T. Südmeyer, R. Paschotta, R. Hövel, M. Moser, S. Erhard, M. Karszewski, A. Giesen, and U. Keller, "16.2-W average power from a diode-pumped femtosecond Yb:YAG thin disk laser," Opt. Lett. **25**(11), 859–861 (2000).
9. C. J. Saraceno, F. Emaury, O. H. Heckl, C. R. E. Baer, M. Hoffmann, C. Schriber, M. Golling, T. Südmeyer, and U. Keller, "275 W average output power from a femtosecond thin disk oscillator operated in a vacuum environment," Opt. Express **20**(21), 23535–23541 (2012).
10. C. J. Saraceno, F. Emaury, C. Schriber, M. Hoffmann, M. Golling, T. Südmeyer, and U. Keller, "Ultrafast thin-disk laser with 80 μJ pulse energy and 242 W of average power," Opt. Lett. **39**(1), 9–12 (2014).

#300918 https://doi.org/10.1364/OE.25.022518
Journal © 2017 Received 29 Jun 2017; revised 18 Aug 2017; accepted 20 Aug 2017; published 7 Sep 2017

Optics EXPRESS

11. A. Giesen, H. Hügel, A. Voss, K. Wittig, U. Brauch, and H. Opower, "Scalable Concept for Diode-Pumped High-Power Solid-State Lasers," Appl. Phys. B **58**(5), 365–372 (1994).
12. U. Keller, K. J. Weingarten, F. X. Kärtner, D. Kopf, B. Braun, I. D. Jung, R. Fluck, C. Hönninger, N. Matuschek, and J. Aus der Au, "Semiconductor saturable absorber mirrors (SESAMs) for femtosecond to nanosecond pulse generation in solid-state lasers," IEEE J. Sel. Top. Quantum Electron. **2**(3), 435–453 (1996).
13. C. M. Heyl, C. L. Arnold, A. Couairon, and A. L'Huillier, "Introduction to macroscopic power scaling principles for high-order harmonic generation," J. Phys. At. Mol. Opt. Phys. **50**(1), 013001 (2017).
14. F. Emaury, A. Diebold, C. J. Saraceno, and U. Keller, "Compact XUV Source at Megahertz Pulse Repetition Rate with a Low-Noise Ultrafast Thin Disk Oscillator," Optica **23**, 980–984 (2015).
15. F. Emaury, C. J. Saraceno, B. Debord, D. Ghosh, A. Diebold, F. Gèrôme, T. Südmeyer, F. Benabid, and U. Keller, "Efficient spectral broadening in the 100-W average power regime using gas-filled kagome HC-PCF and pulse compression," Opt. Lett. **39**(24), 6843–6846 (2014).
16. J. Schulte, T. Sartorius, J. Weitenberg, A. Vernaleken, and P. Russbueldt, "Nonlinear pulse compression in a multi-pass cell," Opt. Lett. **41**(19), 4511–4514 (2016).
17. S. Hädrich, M. Kienel, M. Müller, A. Klenke, J. Rothhardt, R. Klas, T. Gottschall, T. Eidam, A. Drozdy, P. Jójárt, Z. Várallyay, E. Cormier, K. Osvay, A. Tünnermann, and J. Limpert, "Energetic sub-2-cycle laser with 216 W average power," Opt. Lett. **41**(18), 4332–4335 (2016).
18. D. E. Spence, P. N. Kean, and W. Sibbett, "60-fsec pulse generation from a self-mode-locked Ti:sapphire laser," Opt. Lett. **16**(1), 42–44 (1991).
19. J. Brons, V. Pervak, E. Fedulova, D. Bauer, D. Sutter, V. Kalashnikov, A. Apolonskiy, O. Pronin, and F. Krausz, "Energy scaling of Kerr-lens mode-locked thin-disk oscillators," Opt. Lett. **39**(22), 6442–6445 (2014).
20. J. Brons, V. Pervak, D. Bauer, D. Sutter, O. Pronin, and F. Krausz, "Powerful 100-fs-scale Kerr-lens mode-locked thin-disk oscillator," Opt. Lett. **41**(15), 3567–3570 (2016).
21. K. Beil, S. T. Fredrich-Thornton, F. Tellkamp, R. Peters, C. Kränkel, K. Petermann, and G. Huber, "Thermal and laser properties of Yb:LuAG for kW thin disk lasers," Opt. Express **18**(20), 20712–20722 (2010).
22. T. Südmeyer, C. Kränkel, C. R. E. Baer, O. H. Heckl, C. J. Saraceno, M. Golling, R. Peters, K. Petermann, G. Huber, and U. Keller, "High-power ultrafast thin disk laser oscillators and their potential for sub-100-femtosecond pulse generation," Appl. Phys. B **97**(2), 281–295 (2009).
23. F. Brunner, T. Südmeyer, E. Innerhofer, F. Morier-Genoud, R. Paschotta, V. E. Kisel, V. G. Shcherbitsky, N. V. Kuleshov, J. Gao, K. Contag, A. Giesen, and U. Keller, "240-fs pulses with 22-W average power from a mode-locked thin-disk Yb:KY(WO$_4$)$_2$ laser," Opt. Lett. **27**(13), 1162–1164 (2002).
24. O. H. Heckl, C. Kränkel, C. R. E. Baer, C. J. Saraceno, T. Südmeyer, K. Petermann, G. Huber, and U. Keller, "Continuous-wave and modelocked Yb:YCOB thin disk laser: first demonstration and future prospects," Opt. Express **18**(18), 19201–19208 (2010).
25. C. J. Saraceno, O. H. Heckl, C. R. E. Baer, C. Schriber, M. Golling, K. Beil, C. Kränkel, T. Südmeyer, G. Huber, and U. Keller, "Sub-100 femtosecond pulses from a SESAM modelocked thin disk laser," Appl. Phys. B **106**(3), 559–562 (2012).
26. C. Schriber, L. Merceron, A. Diebold, F. Emaury, M. Golling, K. Beil, C. Kränkel, C. J. Saraceno, T. Südmeyer, and U. Keller, "Pushing SESAM modelocked thin-disk lasers to shortest pulse durations," in *Advanced Solid State Lasers*, OSA Technical Digest (online) (Optical Society of America, 2014), AF1A.4.
27. C. Kränkel, "Rare-earth doped sesquioxides for diode-pumped high power lasers in the 1-, 2-, and 3-µm spectral range," IEEE J. Sel. Top. Quant. **21**(1), 1602013 (2015).
28. R. Peters, C. Kränkel, S. T. Fredrich-Thornton, K. Beil, O. H. Heckl, C. R. E. Baer, C. J. Saraceno, T. Südmeyer, U. Keller, K. Petermann, and G. Huber, ""Thermal analysis and efficient high power continuous-wave and mode-locked thin disk laser operation of Yb-doped sesquioxides," Appl. Phys," B-Lasers Opt. **102**(3), 509–514 (2011).
29. P. A. Loiko, K. V. Yumashev, R. Schödel, M. Peltz, C. Liebald, X. Mateos, B. Deppe, and C. Kränkel, "Thermo-optic properties of Yb:Lu_2O_3 single crystals," Appl. Phys. B **120**(4), 601–607 (2015).
30. R. Wynne, J. L. Daneu, and T. Y. Fan, "Thermal coefficients of the expansion and refractive index in YAG," Appl. Opt. **38**(15), 3282–3284 (1999).
31. R. Peters, C. Kränkel, K. Petermann, and G. Huber, "Broadly tunable high-power Yb:Lu$_{(2)}$O$_{(3)}$ thin disk laser with 80% slope efficiency," Opt. Express **15**(11), 7075–7082 (2007).
32. C. R. E. Baer, C. Kränkel, C. J. Saraceno, O. H. Heckl, M. Golling, R. Peters, K. Petermann, T. Südmeyer, G. Huber, and U. Keller, "Femtosecond thin-disk laser with 141 W of average power," Opt. Lett. **35**(13), 2302–2304 (2010).
33. C. J. Saraceno, S. Pekarek, O. H. Heckl, C. R. E. Baer, C. Schriber, M. Golling, K. Beil, C. Kränkel, G. Huber, U. Keller, and T. Südmeyer, "Self-referenceable frequency comb from an ultrafast thin disk laser," Opt. Express **20**(9), 9650–9656 (2012).
34. C. J. Saraceno, C. Schriber, O. H. Heckl, C. R. E. Baer, M. Golling, K. Beil, C. Kränkel, G. Huber, and U. Keller, "25 W, 185 fs Pulses from an Yb:Lu_2O_3 Modelocked Thin Disk Laser.," in *Europhoton 2012—5th EPS-QEOD Europhoton Conference*, 2012)
35. C. R. E. Baer, O. H. Heckl, C. J. Saraceno, C. Schriber, C. Kränkel, T. Südmeyer, and U. Keller, "Frontiers in passively mode-locked high-power thin disk laser oscillators," Opt. Express **20**(7), 7054–7065 (2012).

Optics EXPRESS

36. B. Kreipe, J. Andrade, B. Deppe, C. Kränkel, and U. Morgner, "Kerr-lens mode-locked Yb^{3+}:Lu_2O_3 thin-disk laser," in *Conference on Lasers and Electro-Optics, OSA Technical Digest (2016) (Optical Society of America*, 2016), paper SM1I.4.
37. C. Paradis, N. Modsching, V. J. Wittwer, B. Deppe, C. Kränkel, and T. Südmeyer, "Generation of 35-fs pulses from a Kerr lens mode-locked Yb:Lu_2O_3 thin-disk laser," Opt. Express **25**(13), 14918–14925 (2017).
38. V. Peters, A. Bolz, K. Petermann, and G. Huber, "Growth of high-melting sesquioxides by the heat exchanger method," J. Cryst. Growth **237–239**, 879–883 (2002).
39. J. Neuhaus, J. Kleinbauer, A. Killi, S. Weiler, D. Sutter, and T. Dekorsy, "Passively mode-locked Yb:YAG thin-disk laser with pulse energies exceeding 13 microJ by use of an active multipass geometry," Opt. Lett. **33**(7), 726–728 (2008).
40. V. Magni, "Multielement stable resonators containing a variable lens," J. Opt. Soc. Am. A **4**(10), 1962–1969 (1987).
41. C. J. Saraceno, O. H. Heckl, C. R. E. Baer, M. Golling, T. Südmeyer, K. Beil, C. Kränkel, K. Petermann, G. Huber, and U. Keller, "High damage threshold SESAMs for high power femtosecond modelocking: 23 W, 235 fs Yb:LuScO3 thin-disk laser," in *CLEO Europe 2011* (2011).
42. C. J. Saraceno, F. Emaury, C. Schriber, A. Diebold, M. Hoffmann, M. Golling, T. Südmeyer, and U. Keller, "Toward millijoule-level high-power ultrafast thin-disk oscillators," IEEE J. Sel. Top. Quant. **1**, 1100318 (2015).
43. A. Diebold, F. Emaury, C. Schriber, M. Golling, C. J. Saraceno, T. Südmeyer, and U. Keller, "SESAM mode-locked Yb:$CaGdAlO_4$ thin disk laser with 62 fs pulse generation," Opt. Lett. **38**(19), 3842–3845 (2013).
44. R. Grange, M. Haiml, R. Paschotta, G. J. Spuhler, L. Krainer, M. Golling, O. Ostinelli, and U. Keller, "New regime of inverse saturable absorption for self-stabilizing passively mode-locked lasers," Appl. Phys. B **80**(2), 151–158 (2005).
45. T. R. Schibli, E. R. Thoen, F. X. Kärtner, and E. P. Ippen, "Suppression of Q-switched mode locking and break-up into multiple pulses by inverse saturable absorption," Appl. Phys. B **70**(S1), S41–S49 (2000).
46. M. Haiml, R. Grange, and U. Keller, "Optical characterization of semiconductor saturable absorbers," Appl. Phys. B **79**(3), 331–339 (2004).
47. R. Peters, "Ytterbium-dotierte Sesquioxide als hocheffiziente Lasermaterialien," PhD-Thesis (Universität Hamburg, Germany, 2009).
48. R. Paschotta, J. Aus der Au, G. J. Spühler, S. Erhard, A. Giesen, and U. Keller, "Passive mode locking of thin disk lasers: effects of spatial hole burning," Appl. Phys. B **72**(3), 267–278 (2001).
49. C. G. E. Alfieri, D. Waldburger, S. M. Link, E. Gini, M. Golling, G. Eisenstein, and U. Keller, "Optical efficiency and gain dynamics of modelocked semiconductor disk lasers," Opt. Express **25**(6), 6402–6420 (2017).
50. B. C. Stuart, M. D. Feit, A. M. Rubenchik, B. W. Shore, and M. D. Perry, "Laser-induced damage in dielectrics with nanosecond to subpicosecond pulses," Phys. Rev. Lett. **74**(12), 2248–2251 (1995).
51. C. G. E. Alfieri, A. Diebold, F. Emaury, E. Gini, C. J. Saraceno, and U. Keller, "Improved SESAMs for femtosecond pulse generation approaching the kW average power regime," Opt. Express **24**(24), 27587–27599 (2016).
52. A. Diebold, T. Zengerle, C. G. E. Alfieri, C. Schriber, F. Emaury, M. Mangold, M. Hoffmann, C. J. Saraceno, M. Golling, D. Follman, G. D. Cole, M. Aspelmeyer, T. Südmeyer, and U. Keller, "Optimized SESAMs for kilowatt-level ultrafast lasers," Opt. Express **24**(10), 10512–10526 (2016).

1. Introduction

Ultrafast laser sources are the workhorse of a variety of scientific and industrial applications. The diversity of available technologies and attractive performance of these table-top systems can be deployed in fundamental research experiments, new medical procedures, or high-precision micro-machining [1–3]. High-power ultrafast laser systems delivering intense infrared laser pulses are of particular interest for efficient frequency conversion up to the extreme-ultraviolet (XUV) spectral region via high-harmonic generation (HHG). The high repetition rate and high photon flux achievable through this approach can significantly reduce the acquisition time and improve the signal-to-noise ratio (SNR) of attosecond experiments [4].

The state-of-the-art of high-power ultrafast laser sources is demonstrated by amplifier systems based on the thin-disk, fiber or Innoslab technology, reaching kW-level average powers with peak powers exceeding the GW level [5–7]. However, the impressive performance of these laser amplifier systems comes at the cost of a high system complexity and, in some cases, non-diffraction-limited beam quality. Modelocked thin-disk laser oscillators are an attractive alternative to the complex amplifier systems and combine high output power and high peak power in a compact table-top MHz oscillator with excellent beam quality. Passive modelocking of a diode-pumped thin-disk laser (TDL) was demonstrated for the first time in 2000 [8] and currently represents the state-of-the-art of sub-picosecond

Optics EXPRESS

ultrafast oscillators, reaching average output powers up to 275 W (583 fs) [9], pulse energies up to 80 µJ (1.1 ps) [10] and peak powers up to 66 MW [10] [Fig. 1(a)]. The power scalability of the thin-disk geometry [11] and SESAM modelocking [12], combined with the continuous improvement of the thin-disk crystal quality and contacting technique, opens prospects of kW-level modelocked TDLs at picosecond pulse durations. However, shorter pulse durations are important for efficient HHG [13,14]. Several nonlinear compression techniques have been demonstrated at high average and peak-power to shorten the pulse duration [14–17]. Nevertheless, since only limited compression factors can be achieved in these schemes, short pulses directly out of the laser oscillator are needed to reach few-cycle pulses after a single compression stage.

Reducing the pulse duration of modelocked TDLs is therefore an ongoing challenge. Kerr-lens modelocked (KLM) [18] thin-disk oscillators have approached a similar 270-W average power as SESAM-modelocked TDLs with the advantage of a shorter 330-fs pulse duration, as expected from a faster saturable absorber [19]. Even shorter pulses of 140 fs were achieved with 155 W of average power and a peak power of 62 MW [20]. However, KLM comes with a severe trade-off because the fast saturable absorber requires a strong coupling between resonator design and soliton pulse formation, and pushes the laser cavity to the edge of its stability regime. Thus, KLM lasers have had a limited impact for industrial lasers as they are highly alignment-sensitive and less flexible to operating over a wide range of output parameters than SESAM-modelocked lasers. In particular, energy scaling to >15 µJ remains to be demonstrated.

To date, the power scaling of modelocked TDLs has relied extensively on the high-quality gain material Yb:YAG, benefiting from its mature growth technology and wide availability. Yet, high-power SESAM-modelocked Yb:YAG TDLs are operating at pulse durations >500 fs mainly due to the limited gain bandwidth of Yb:YAG (8 nm full-width at half maximum (FWHM) [21]). Alternative broadband gain materials suitable for the thin-disk geometry are actively pursued in order to access the high-power sub-100-fs regime directly from the oscillator [Figs. 1(a) and 1(b)] [22]. Early investigations of short-pulsed SESAM-modelocked TDLs based on Yb-doped tungstate or borate materials demonstrated pulse durations <300 fs at power levels up to 22 W [23,24]. First sub-100-fs modelocking was then achieved with Yb:$LuScO_3$, a material from the cubic sesquioxides family, with 5 W of average power and 96-fs pulses [25]. In recent years, the ultra-broadband gain material Yb:CALGO (Yb:$CaGdAlO_4$), allowed for even shorter pulse durations but at the expense of average output power, i.e. as short as 49 fs at 2-W average power [26].

Amongst these broadband materials, the Yb-doped sesquioxide lutetia Yb:Lu_2O_3 (Yb:LuO) is potentially an ideal candidate material to combine high average powers comparable to Yb:YAG but at significantly shorter pulse durations. This cubic material benefits from excellent thermal properties, with a thermal conductivity close to twice that of Yb:YAG at typical doping concentrations (κ_{LuO} = 12 W/(m·K) and κ_{YAG} = 7 W/(m·K) for an Yb doping density of $8 \cdot 10^{20}$ cm^{-3} [27,28]), and a broad emission bandwidth supporting sub-100-fs pulses [12.5 nm FWHM [27], see Fig. 1(b)]. Furthermore, Yb:LuO has smaller thermo-optic and thermal expansion coefficients than Yb:YAG [29,30]. These advantageous properties, together with demonstrated slope efficiencies >80% [31], make Yb:LuO an attractive candidate for high-power ultrashort-pulsed laser operation.

Optics EXPRESS

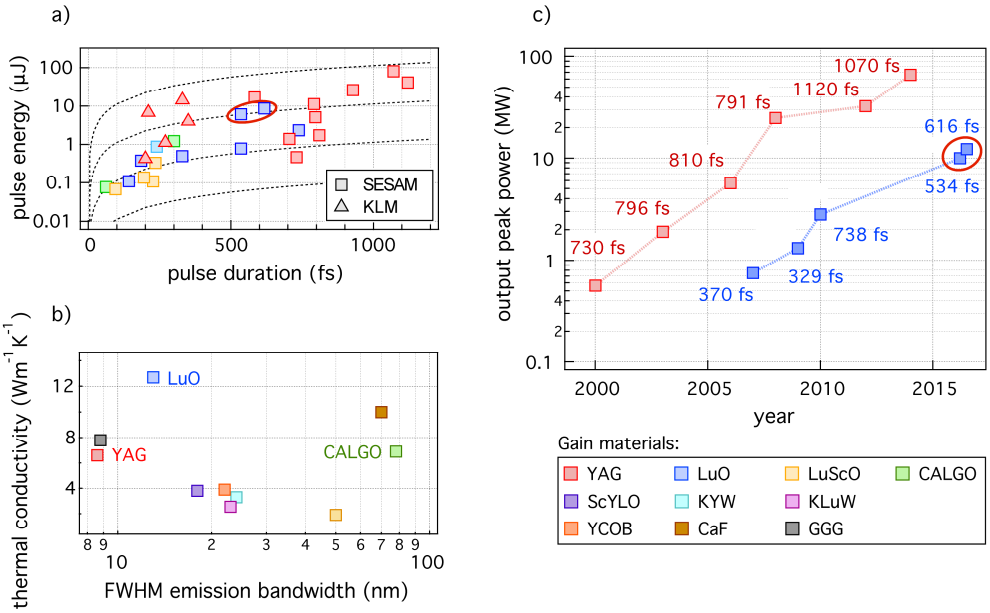

Fig. 1. a) Overview of the results demonstrated from modelocked TDLs with different Yb-doped gain materials. Results presented in this paper are indicated by the red circles. b) Thermal conductivity and emission bandwidth of gain materials suitable for the thin-disk geometry. The thermal conductivity is given for a typical Yb doping density of 8×10^{20} cm^{-3}. c) Evolution of the performance of SESAM-modelocked Yb:YAG and Yb:LuO TDLs.

High-power modelocked operation with Yb:LuO has been demonstrated in a SESAM-modelocked TDL up to 141 W of average output power with relatively long 738-fs pulses at a repetition rate of 60 MHz [32]. Short-pulse operation was also achieved down to 140 fs at a limited power level of 7 W and a repetition rate of 64 MHz [33]. Average power scaling to 25 W was demonstrated with 185-fs pulses [34], which remains to date the highest average power achieved from a SESAM-modelocked TDL at sub-200-fs pulse durations. These promising results, however, were all obtained at high repetition rates and consequently limited output peak powers below 3 MW. The Yb:LuO disks available at the time of these experiments were comparatively thick (150 – 250 µm) and contacted on copper-alloy heatsinks, which resulted in significant thermal lensing [32,35]. Recently, the first Kerr-lens modelocking of an Yb:LuO TDL was demonstrated with an average power of 6 W and 165-fs pulses at a repetition rate of 60 MHz [36]. First sub-100-fs pulse generation from an Yb:LuO TDL was then achieved in a 61-MHz KLM oscillator with up to 11 W of average power and 88-fs pulses or with pulses as short as 35 fs at <2-W power level [37]. These results, however, were also limited to output peak powers below 2 MW.

Here, we present the first high peak power SESAM-modelocked Yb:LuO TDL reaching peak powers in excess of 10 MW [see Fig. 1(c)], with average powers up to 90 W and pulse durations close to 500 fs at repetition rates below 15 MHz. To achieve these results, we designed a new set of Yb:LuO disks with reduced thickness below 150 µm, optimized crystal quality, and contacted on diamond for enhanced thermal management. These improvements allowed us to increase the cavity length compared to prior results and scale up the peak power of femtosecond Yb:LuO TDLs. After presenting the modelocking results (section 2), we identify the current challenges of high peak-power SESAM-modelocking and present our numerical model, validated by experimental results, providing a criterion for stable modelocking (section 3). Finally, we use our model as a tool to determine the cavity and SESAM design requirements for accessing the 100-W average power, 200-fs regime, with peak-powers approaching 100 MW.

Optics EXPRESS

2. High-peak-power SESAM-modelocked Yb:LuO TDL

In this section, we present our high-peak-power (>10 MW) Yb:LuO modelocking results. To enable this performance, a new high-quality thin-disk was used. We chose Yb:LuO for its advantageous thermal properties and comparatively large bandwidth as discussed in the introduction. The crystal, from which the large-area (∅ 12 mm) 110-µm-thick Yb:LuO disk was prepared, was grown at the Institut für Laser-Physik of the Universität Hamburg by the heat exchanger method (HEM) [38]. It has a doping concentration of 3 at.% (Yb-ion density of ≈ 8.6 × 10^{20} cm^{-3}). The disk was contacted onto a diamond heatsink (TRUMPF Laser GmbH) and has a cold radius of curvature (ROC) of −2.2 m, free of astigmatism. The disk was mounted within a 36-pass thin-disk laser head (TRUMPF Laser GmbH) and pumped into the zero-phonon line (ZPL) at 976 nm with a pump spot diameter of 2.5 mm. The narrow-linewidth pump diode (DILAS Diodenlaser GmbH) is wavelength-stabilized with a volume Bragg grating (VBG). The cooling water temperature for the diode stacks was adjusted to achieve optimum locking of the pump power into the VBG line at 400 W. Under these conditions, the pump absorption efficiency is above 96% for the targeted pump power range, at typical TDL inversion levels (<20%). The additional thermal lensing of the disk was measured up to the highest pump intensity of 8 kW/cm^2 and remained below 0.06 m^{-1} (7% of the cold disk focal power) as well as radially symmetric. This low thermal lensing of the disk, combined to operation of the oscillator within a pressure-controlled environment, allowed us to substantially increase the pulse energy and peak power compared to previous Yb:LuO results.

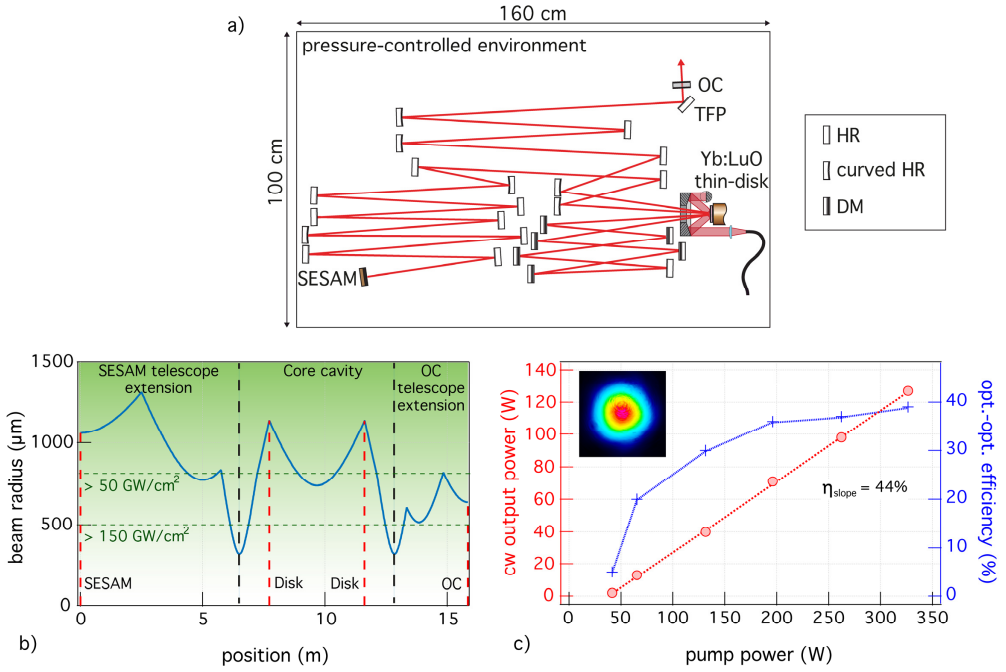

Fig. 2. a) Illustration of the full 9.5-MHz cavity layout in the pressure-controlled chamber. OC: output coupler, TFP: thin-film polarizer, HR: highly-reflective mirror, DM: dispersive mirror. b) Cavity mode radii for single transverse mode operation. The basic cavity defining the modal overlap of the laser and pump beams on the disk is extended with two 4f-telescope extensions. No optics are used within the region where peak intensities >150 GW/cm^2 are expected. HR mirrors and DMs are introduced where the expected peak intensities are <150 GW/cm^2 and <50 GW/cm^2, respectively. c) Continuous-wave (cw) output power slope with an OC transmission of 8.4% at a pressure of 1 mbar. Inset: Measured mode profile at the maximum output power of 127 W.

Optics EXPRESS

The resonator design is based on a simple core cavity consisting of two flat end mirrors, the thin-disk and a concave curved mirror (CM) with a ROC of −5 m, replicated once to introduce a second double-reflection through the disk per cavity roundtrip. This 8-pass approach increases the effective gain available from the very thin disk and allows for operation at higher output coupler (OC) transmission values [39]. The core cavity is designed to have a laser mode radius that amounts to 91% of the pump mode radius on the Yb:LuO disk and to operate in the center of the stability region [40]. The cavity length is then extended by introducing telescope extensions at both ends of the cavity. An illustration of the cavity layout is given in Fig. 2(a). The cavity extensions are designed to increase the overall mode diameters in the laser resonator in order to reduce the intensity on the intracavity optics and the fluence on the SESAM in high-power operation. To avoid damaging the intracavity optics during or prior to initiating modelocking, we set conservative upper bounds for the maximum peak intensities allowed on these elements during modelocked operation. We choose upper bounds of 150 GW/cm^2 for the highly-reflective (HR) mirrors and 50 GW/cm^2 for the dispersive mirrors (DMs). Based on the expected intracavity parameters (average powers <2 kW, peak powers <500 MW), these bounds imply minimum laser spot sizes of 500 µm for the HRs and 800 µm for the DMs [Fig. 2(b)]. A thin-film polarizer (TFP) is inserted in the cavity for polarization selection and the oscillator is set up in a pressure-controlled chamber as in [9]. In this configuration and with an OC transmission of 8.4%, single transverse mode operation is achieved with >120 W of cw output power, at an optical-to-optical efficiency of 39% and a slope efficiency of 44% [Fig. 2(c)] at a pressure of 1 mbar. The measured M^2-values in cw operation of M^2_x = 1.01 and M^2_y = 1.03 indicate close to diffraction-limited beam quality at ambient pressure, as well as at the minimum pressure of 1 mbar, limited by our vacuum pump.

For initiating and stabilizing modelocked operation, we introduce into the cavity a large-area semiconductor saturable absorber mirror (SESAM) optimized for high-damage threshold following our guidelines in [41]. The as-grown semiconductor structure is top-coated with three pairs of dielectric layers, leading to a high saturation fluence of F_{sat} = 120 µJ/cm^2 and a high rollover coefficient of $F_{2,\ 1\ ps}$ = 5 J/cm^2 (measured for a 1-ps pulse), together with a moderate modulation depth of ΔR = 1.1%, low nonsaturable losses of ΔR_{ns} = 0.05% and a recovery time of $\tau_{1/e}$ = 6 ps. A measurement of the SESAM nonlinear reflectivity curve, as well as a complete description of the epitaxial structure, is given in [42]. The SESAM is contacted onto a copper substrate and mounted on a water-cooled aluminum mount equipped with a Peltier element for active temperature control. The temperature of the SESAM was set to 18 °C.

The nonlinear phase shift required for soliton pulse formation is fine-tuned by varying the residual air pressure within the chamber. Intracavity negative dispersion (D_{rt}) required to balance this nonlinear phase is adjusted by introducing dispersive mirrors in the cavity. Note that a reflective TFP typically presents a non-negligible negative group-delay dispersion (GDD), in our case measured to be ≈ -500 fs^2. First high-peak-power modelocking was achieved with an intracavity dispersion of –4100 fs^2 per roundtrip and a residual air pressure (p_{atm}) of 15 mbar in a 14.8 MHz cavity without OC extension. Stable single-pulse modelocked operation was obtained up to 90 W of average power at a pulse duration of 534 fs. The output pulse energy was 6.1 µJ resulting in a peak power of 10.1 MW.

To further scale the output pulse energy and peak power, the OC extension was added to the cavity [see Fig. 2(b)]. The intracavity dispersion was adjusted to –7400 fs^2 per roundtrip by introducing additional dispersive mirrors and the chamber was evacuated to the minimum residual air pressure of 1 mbar. Stable single-pulse modelocked operation was achieved up to 82 W of average power at a pulse duration of 616 fs and a repetition rate of 9.5 MHz [see Fig. 3]. The pulse energy was 8.6 µJ, resulting in a peak power of 12.3 MW. These are the highest pulse energies and peak powers achieved from a modelocked TDL based on Yb:LuO. The resulting parameters are summarized in Table 1.

Optics EXPRESS

Table 1. Laser parameters of the presented modelocking results

$P_{pk,\,out}$	D_{rt}	p_{atm}	f_{rep}	P_{avg}	τ_p	$E_{p,\,out}$
10.1 MW	–4100 fs^2	15 mbar	14.8 MHz	90 W	534 fs	6.1 µJ
12.3 MW	–7400 fs^2	1 mbar	9.5 MHz	82 W	616 fs	8.6 µJ

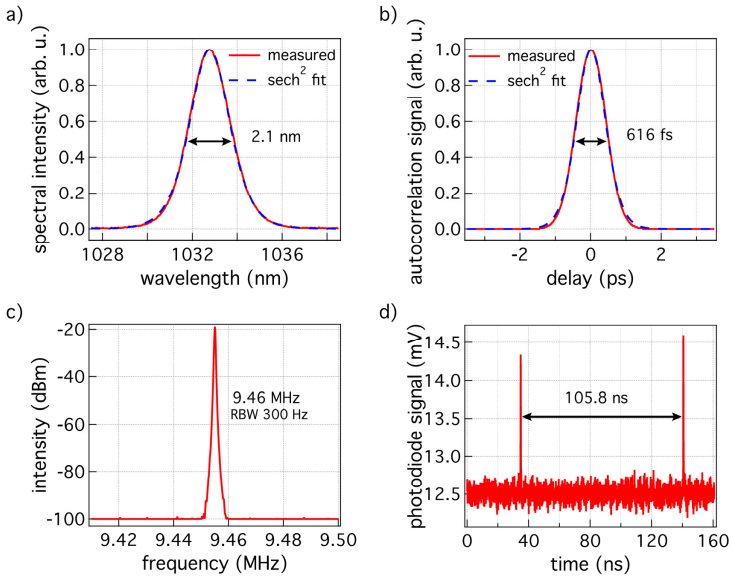

Fig. 3. SESAM-modelocked Yb:LuO TDL with the record-high 12.3-MW peak power result: a) Optical spectrum of the 616-fs pulses, with a FWHM of 2.1 nm. b) Autocorrelation trace of the nearly transform-limited 616-fs pulses (time-bandwidth product (TBP) of 0.362). The delay was scanned over a long range of 60 ps and no double-pulsing was observed. c) Microwave spectrum analyzer signal showing modelocking at a repetition rate of 9.46 MHz with a SNR >70 dB (resolution bandwidth RBW of 300 Hz over a span of 90 kHz) d) Signal acquired on a fast sampling scope from a fast photodiode (45 GHz) showing single-pulse modelocking with the corresponding roundtrip time of 105.8 ns.

In particular, these results represent the first demonstration of a high-peak-power Yb:LuO TDL reaching peak-powers in excess of 10-MW. The superior quality of the new thin-disk used for these experiments enabled the implementation of a multipass geometry as well as operation at a reduced ambient pressure. This allowed for high intracavity peak-powers up to 185 MW with reduced nonlinear phase-shifts (~50 mrad) for soliton pulse shaping. The resulting low amount of required negative intracavity dispersion allowed for the use of only a few DMs with low GDD values, which mitigated the thermal issues we often observe with such mirrors [42]. No damage of the SESAM was observed during our optimization of the cw-modelocking regime. However further peak-power scaling was limited by the onset of instabilities at higher powers and shorter pulse durations, such as double-pulsing and modal instabilities, which will be addressed in the next section.

3. Numerical modeling of high-peak-power SESAM-modelocked TDLs

As observed in our present peak-power scaling experiments and in prior work on short-pulsed SESAM-modelocked TDLs [25,33,43], modelocked operation at high pulse energies and short pulse durations is limited by the onset of modelocking instabilities or modal instabilities (i.e. beam quality degradation). These limitations can be explained by considering the combined effect of the finite gain bandwidth (GBW) of the thin-disk material and of the reflectivity rollover happening in the SESAM at high intensities, which can be interpreted as an inverse saturable absorption (ISA) effect [44]. Within a laser cavity, these two effects lead on the one hand to a reduction of the loss modulation provided by the SESAM at the highest

Optics EXPRESS

pulse energies and/or shortest pulse durations, which can favor double-pulsing or cw-breakthroughs, and on the other hand to increased absorption losses in the SESAM, which increase the heat load on the SESAM and introduce thermal lensing. In this section, we present a numerical model for calculating the net cavity gain of a modelocked TDL which accounts for the finite gain bandwidth and the SESAM inverse saturable absorption.

3.1 SESAM reflectivity within a modelocked laser cavity

The nonlinear reflectivity of a SESAM increases with increasing pulse fluence due to saturable absorption (SA) in the absorber layers of the epitaxial structure, in our case InGaAs quantum wells (QWs). In the absence of parasitic effects such as two photon absorption (TPA) and for sufficiently large fluences, the SESAM reflectivity would asymptotically reach a maximum, as illustrated in Fig. 4 (no TPA). However, for large pulse fluences and intensities, TPA or free-carrier absorption lead to inverse saturable absorption, i.e. a rollover of the SESAM reflectivity [44,45] [see Fig. 4 (TPA at fixed τ_p)]. The usual model-function for the reflectivity of a SESAM is given by [46]:

$$R(F) = R_{SA}(F) \cdot R_{ISA}(F) = R_{ns} \frac{\ln[1 + R_{lin} / R_{ns} (e^{F/F_{sat}} - 1)]}{F / F_{sat}} \cdot e^{-F/F_2} \quad (1)$$

where $R_{lin} = 1 - \Delta R - \Delta R_{ns}$, is the cw nonsaturated SESAM reflectivity and $R_{ns} = 1 - \Delta R_{ns}$, is the maximum SESAM reflectivity in the absence of ISA. F, F_{sat} and F_2 are the pulse fluence, the SESAM saturation fluence and inverse saturation fluence respectively, while ΔR and ΔR_{ns} (or L_{ns}) denote the modulation depth and SESAM losses in the absence of ISA. The inverse saturation fluence F_2 characterizes the strength of the SESAM reflectivity rollover at high intensities due to ISA. Based on detailed studies [44–46], the SESAM reflectivity rollover is mainly caused by TPA in the fs-regime, taking place especially in the low-bandgap semiconductor materials (GaAs) of the SESAM structure. Therefore, the TPA-induced loss can be represented via a rollover intensity I_2 and the model-function for the SESAM reflectivity can be rewritten as a function of fluence and peak intensity:

$$R(F_p, I_p) = R_{SA}(F_p) \cdot R_{TPA}(I_p) = R_{ns} \frac{\ln[1 + R_{lin} / R_{ns} (e^{F_p/F_{sat}} - 1)]}{F_p / F_{sat}} \cdot e^{-I_p/I_2} \quad (2)$$

where $I_p = 0.88\ F_p / \tau_p$ is the intensity on the SESAM and τ_p is the incident soliton pulse duration. The rollover intensity I_2 only depends on the layer structure of the SESAM. For the case considered here of TPA induced by a soliton pulse, it is related to the inverse saturation fluence F_2, according to [44]:

$$I_2 = 0.88 \frac{F_2}{\tau_p} = \frac{1}{0.665 \int \beta_{TPA}(z) n^2(z) |\varepsilon(z)|^4 \, dz} \quad (3)$$

where $\beta_{TPA}(z)$, $n(z)$ and $\varepsilon(z)$ are the material-dependent TPA coefficient, the refractive index and the normalized electric field at a given position z within the SESAM structure. The distinction between the rollover fluence F_2 and the rollover intensity I_2 is particularly relevant when considering the SESAM reflectivity within a modelocked laser cavity. Due to soliton pulse shaping, the incident pulse duration on the SESAM depends on the pulse energy according to:

Optics EXPRESS

$$\tau_p = 1.76 \frac{2|D_{rt}|}{\gamma_{rt} E_p} \tag{4}$$

where D_{rt} is the total intracavity negative group delay dispersion per roundtrip, $\gamma_{rt} = \phi_{NL,rt} / P_{pk}$ is the total self-phase modulation (SPM) coefficient per roundtrip, $\phi_{NL,rt}$ being the total intracavity nonlinear phase per roundtrip, and E_p is the intracavity pulse energy. Therefore, when the intracavity pulse energy is varied, the SESAM reflectivity effectively follows a curve with constant I_2 [Eq. (2)] but not with constant F_2 [Eq. (1)], as is the case during a measurement of the SESAM reflectivity. As illustrated in Fig. 4, this effectively leads to a more pronounced rollover.

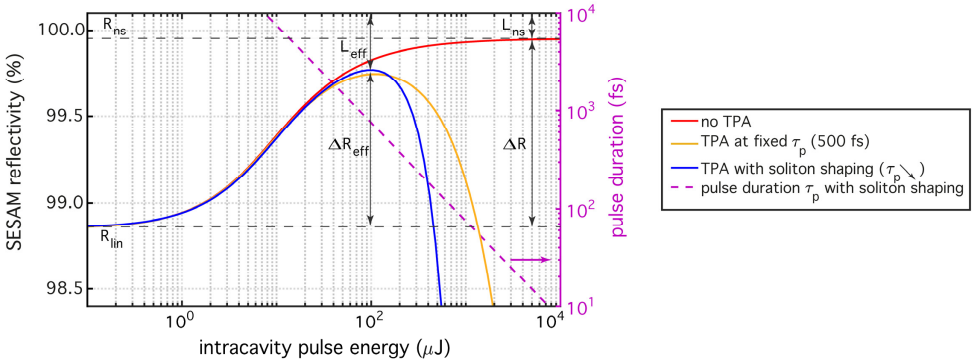

Fig. 4. Simulated nonlinear reflectivity curve of the SESAM used in the modelocking experiments for a waist w_{SESAM} = 1.3 mm, in different cases: without TPA effect (orange), for a fixed F_2 value corresponding to a pulse duration of 500 fs (yellow) and finally accounting for soliton shaping, for a given intracavity dispersion and nonlinearity [see Eq. (4)] (purple). The soliton pulse duration is plotted in a pink dashed line and reaches 500 fs for a pulse energy of 150 μJ. The reduced effective modulation depth and increased losses compared to the specified ΔR and ΔR_{ns} are indicated at the rollover point.

The SESAM reflectivity rollover induced by TPA at high peak intensities leads to the loss modulation provided by the SESAM reaching a maximum value for a given peak intensity. The corresponding intracavity pulse energy is denoted as $E_{p,0}^{SESAM}$. After this rollover point, the SESAM reflectivity decreases rapidly. In the presence of soliton shaping (purple line in Fig. 4), the effective available modulation depth ΔR_{eff} is always smaller and the effective the losses L_{eff} are always larger than the SESAM fit parameters ΔR and ΔR_{ns}, respectively. Thus, for shorter pulses, TPA induces higher SESAM losses, decreases the effective available modulation depth, and shifts the rollover point $E_{p,0}^{SESAM}$ to lower pulse energies. The increased SESAM losses result in a higher thermal load on the SESAM and consequently stronger thermal lensing, which can destabilize the laser cavity. Additionally, the reduced effective modulation depth sets a limit to the minimum achievable pulse duration, as discussed in the next section. To mitigate these effects, it is therefore of high interest to use SESAM structures with reflectivity rollovers shifted to the highest possible peak intensities.

3.2 Finite gain bandwidth: gain reduction at short pulse durations

An important aspect of peak power scaling modelocked oscillators is the ability to use a large fraction of the available gain bandwidth in order to reach the shortest pulse durations with a given gain material. However, as the pulse bandwidth samples a larger fraction of the gain spectrum, the resulting effective gain for the pulse decreases compared to the gain for a cw wave. This gain reduction can be calculated numerically for a given inversion level β. The gain cross-section σ_g reads:

Optics EXPRESS

$$\sigma_g(\nu) = \beta \cdot \sigma_{em}(\nu) - (1-\beta) \cdot \sigma_{abs}(\nu) \tag{7}$$

and the intensity gain G is given by:

$$G(\nu) = N_{dop} n_{passes} \sigma_g(\nu) d_{disk} \tag{8}$$

where $\beta = N_2 / N_{dop}$ is the inversion level, N_2 the inversion population, N_{dop} the Yb-ion density of the disk, σ_{em} and σ_{abs} the emission and absorption cross-sections [47], n_{passes} the number of laser passes in the gain medium per cavity roundtrip, and d_{disk} the thickness of the disk.

In cw operation, we assume a single frequency ν_{cw} lasing at the maximum of the gain spectrum. For a soliton pulse with a spectral bandwidth $\Delta\nu$, the gain is then calculated as:

$$G_p(\Delta\nu) = \int G(\nu) \cdot S\left(\frac{\nu - \nu_{cw}}{\Delta\nu}\right) \cdot d\nu \tag{9}$$

with $S((\nu - \nu_{cw}) / \Delta\nu)$ the normalized sech^2-shaped intensity spectrum of a soliton pulse with a center frequency ν_{cw} and a spectral bandwidth $\Delta\nu$, related to the pulse duration via the time-bandwidth product $\Delta\nu \cdot \tau_p = 0.3148$. We verified that spatial hole burning effects have a negligible impact on the gain for the targeted short pulse durations, and therefore neglect them for simplicity [48].

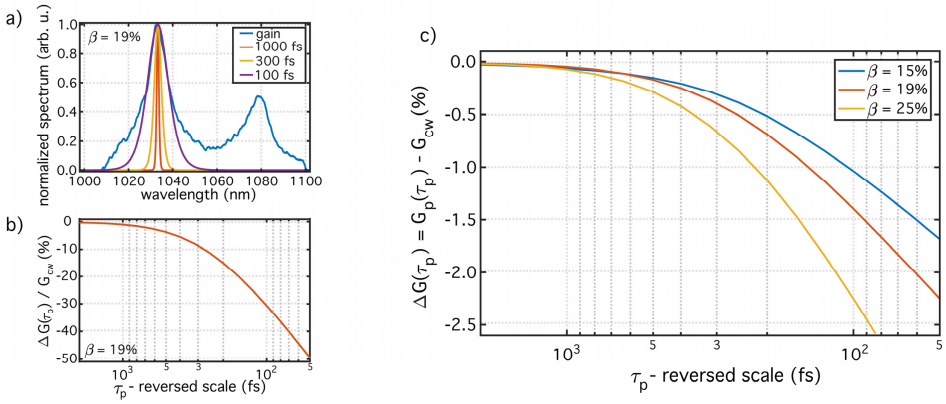

Fig. 5. Simulated reduction of the gain in pulsed operation compared to cw operation for an Yb:LuO TDL. The disk thickness is set to 110 µm and the doping concentration to 3 at.%, as in our experiments. The number of passes of the laser beam through the gain medium is set to 4 per cavity roundtrip, corresponding to a standard V-shaped cavity with a single double-reflection of the laser beam through the disk per roundtrip. Spatial hole burning (SHB) effects, that lead to a reduction of the available gain for long pulse durations [48], were neglected in this calculation. a) Normalized gain spectrum and pulse spectra showing how shorter pulses sample more of the gain cross-section, leading to the reduction in gain. b) Normalized gain reduction for pulsed operation compared to cw operation. c) Absolute gain reduction for pulsed operation compared to cw operation, plotted for increasing inversion levels, corresponding to increasing OC rates.

In Fig. 5, we show relevant characteristics for the gain in an Yb:LuO disk with 110 µm thickness, as used in our experiments. Figure 5(a) shows the gain cross section at 19% inversion. This inversion level is estimated based on the OC transmission and nonsaturated SESAM losses in our experiment. As the pulse duration is reduced, the increase in bandwidth means that gain for the pulse is reduced relative to cw light, as shown in Fig. 5(b). This normalized reduction is largely inversion-independent. Figure 5(c) shows the absolute difference in gain for several values of inversion in our Yb:LuO disk. Since a lower value for the OC transmission is constrained by the need to avoid excessive intracavity powers, this

Optics EXPRESS

absolute difference in gain values is important and can be compared to the available modulation depth of the SESAM: a modulation depth at least as large is required to favor pulsed operation.

3.3 Modelocking stability at high peak-powers: validation of our numerical model on peak-power scaling experiments

In order to find the conditions required to achieve stable modelocking at high peak powers, i.e. high pulse energies and short pulse durations, we now study the combined effect of the SESAM rollover and finite gain bandwidth in experimental results obtained during our peak-power scaling experiments. Our analysis is based on a set of over 30 modelocking results achieved using the same Yb:LuO disk in various cavity configurations and with different SESAMs. Here, we focus in particular on the two following results:

- high peak-power modelocking with 82 W, 616 fs, 9.5 MHz (detailed in section 2)

- lower power modelocking at shorter pulse duration with 16 W, 268 fs, 47.2 MHz

These results are both at the limit of stable modelocking, i.e. the pulse energy could not be increased further in the experiment without leading to double-pulsing or modal instabilities.

Each laser configuration is defined by a thin disk (in this case, the same Yb:LuO disk), a cavity design including nonlinearity, dispersion and a given OC, and a SESAM. As recently demonstrated for modelocked semiconductor disk lasers [49], the quantity $G - L$, defined as the net roundtrip cavity gain, represents a useful tool to investigate the possible modelocking points and the limits of stable modelocked operation in a given laser configuration. We therefore calculate the net cavity gain as a function of the intracavity pulse energy for several different cases, as shown in Fig. 6. Our numerical model calculates as follows:

First, the cw losses are set by the OC transmission and the nonsaturated SESAM losses. The rate equations are then solved for steady-state, single frequency cw operation and the corresponding inversion level β is calculated. The same inversion level is used for all of the curves on the figure. Given this value, we then calculate $G - L$ with respect to cw operation for the following cases, see Fig. 6:

- cw operation (labeled ‘cw’): the cw gain G_{cw} is given by Eqs. (7)–(8), and equals the cw losses.

- Pulsed operation, assuming no rollover effects (labeled ‘no TPA’): the losses are set by the OC transmission and the saturated SESAM losses, assuming no rollover due to TPA (infinite I_2). The pulsed gain equals the cw gain, i.e. assuming infinite gain bandwidth.

- Pulsed operation, assuming infinite gain bandwidth and fixed rollover fluence F_2 (labeled ‘TPA, fixed τ_p’): the losses are set by the OC transmission and the saturated SESAM losses for a fixed rollover fluence F_2 [Eq. (1)], calculated for the pulse duration at the considered modelocking point. The pulsed gain equals the cw gain as in the previous case.

- Pulsed operation, assuming infinite gain bandwidth but including soliton pulse formation for the SESAM response (labeled ‘TPA, soliton shaping’): the losses are set by the OC transmission and the saturated SESAM losses, now considering the soliton pulse circulating within the cavity with a duration following Eq. (4). The SESAM reflectivity is now a function of incoming fluence and peak intensity as in Eq. (2). The pulsed gain also equals the cw gain in this case.

- Pulsed operation, considering both soliton pulse formation and the finite gain bandwidth (GBW) (labeled ‘TPA, sol. shap. + GBW’): the losses are set by the OC transmission and the saturated SESAM losses, considering soliton pulse formation. The gain is calculated according to Eq. (9), i.e. accounting for the finite gain bandwidth.

Optics EXPRESS

We checked that the losses introduced by reflection of the laser beam on the numerous intracavity optics have a negligible impact on the net cavity gain and therefore neglect them. In all cases, a transverse Gaussian beam shape is accounted for numerically in the SESAM losses calculations, and the inversion level is assumed constant in order to show the influence of the different effects given a realistic inversion level for lasing operation. The SESAM is also considered sufficiently fast (recovery time of a few ps), such that a cw wave potentially growing over a roundtrip time experiences the cw losses and double-pulsing is the first limitation expected to set in.

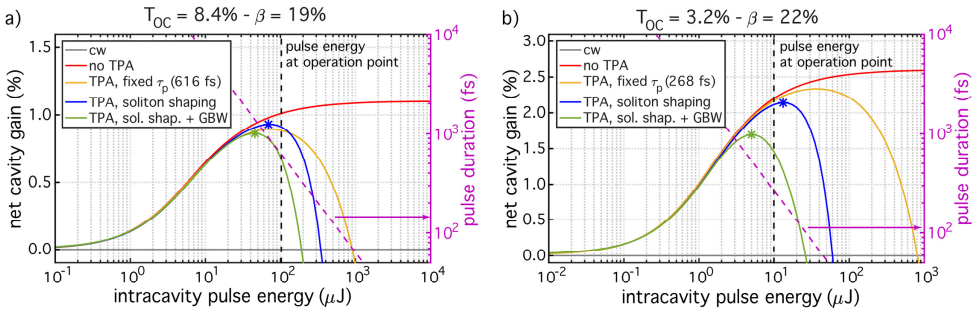

Fig. 6. Net cavity gain for a soliton pulse as a function of the intracavity pulse energy for two different laser configurations: a) high peak-power modelocking (82 W, 616 fs, 9.5 MHz) and b) low power modelocking at shorter pulse duration (16 W, 268 fs, 47.2 MHz). The different cases are listed in the text. The maximum experimental operation point before the onset of instabilities is indicated by the black dashed line. The maximum of the green curve ($E_{p,0}^{cav}$) and the purple curve ($E_{p,0}^{SESAM}$) are indicated by a marker.

In the 616-fs configuration [Fig. 6(a)], the modelocked operation point is only slightly into the rollover of the SESAM reflectivity assuming only soliton pulse shaping (purple line), however the limited gain bandwidth adds an additional rollover contribution and shifts the operation point further into the overall cavity rollover (green line). The contribution of the gain bandwidth rollover is even more pronounced for the 268-fs configuration [Fig. 6(b)]: in this case, the modelocked operation point would actually be close to the optimum operation point for the SESAM reflectivity if only soliton pulse shaping was considered (purple line). In order to explain the limitations and optimize modelocking in this short-pulse regime, it is thus crucial to consider the effect of the finite gain bandwidth in addition to the SESAM rollover, while accounting for soliton shaping to determine the pulse duration.

The optimum operation point maximizing the gain advantage for pulsed operation is located at the maximum of the overall net cavity gain curve (i.e. accounting for soliton pulse shaping and the finite gain bandwidth, green lines). The corresponding pulse energy is denoted as $E_{p,0}^{cav}$. As can be seen from comparing Figs. 6(a) and 6(b), as the targeted pulse duration gets shorter, and therefore the gain bandwidth rollover gets stronger, this point $E_{p,0}^{cav}$ is shifted to lower energies, away from the optimum operation point for the SESAM $E_{p,0}^{SESAM}$, leading to additional SESAM losses. It is therefore of interest to study how far within the overall cavity rollover stable modelocked operation can be achieved, in order to operate with minimum saturated SESAM losses.

In Fig. 7(a), the experimental operation points of over 30 different laser configurations realized during our peak-power scaling experiments are compared to the simulated optimum $E_{p,0}^{cav}$ in each case. The results show that with reasonable accuracy, the maximum operation point leading to stable modelocking is ≈ 2 $E_{p,0}^{cav}$. This is consistent with the experimentally observed appearance of double-pulsing, since in these conditions two pulses with half the energy of the soliton pulse would experience a higher gain due to the cavity rollover.

Optics EXPRESS

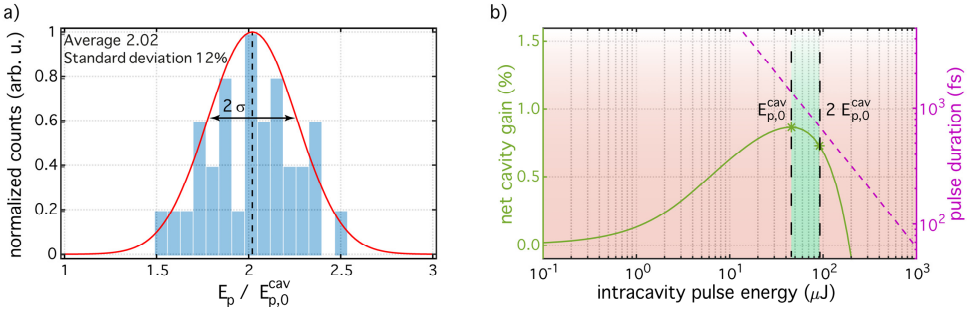

Fig. 7. a) Comparison of the maximum operation point achieved before modelocking instabilities occur, in different laser configurations based on the same Yb:LuO disk. The maximum achievable pulse energy appears to be about twice the pulse energy $E_{p,0}^{cav}$ corresponding to the optimum cavity net gain. b) Illustration of the optimum stable modelocking region. For a given laser configuration, the net cavity gain is calculated accounting for soliton pulse shaping and the finite gain bandwidth. Stable modelocking within the overall cavity rollover is possible, and even desirable to minimize the SESAM saturated losses, at pulse energies up to 2 $E_{p,0}^{cav}$.

Consequently, optimizing the modelocking operation point at short pulse durations is a trade-off between operating close to the maximum of the overall net cavity gain curve, with maximum robustness to modelocking instabilities, and operating close to the maximum of the SESAM reflectivity, with minimum saturated SESAM losses. According to our study, operation within the overall cavity rollover is possible up to a pulse energy $E_{p,max} \approx 2\ E_{p,0}^{cav}$ before modelocking instabilities occur.

To summarize, the optimum region for stable modelocking is determined by calculating the net cavity gain for pulsed operation, accounting for soliton pulse shaping and the finite gain bandwidth, and retrieving the pulse energy $E_{p,0}^{cav}$ corresponding to its maximum. Stable modelocked operation is possible up to a pulse energy twice higher than this optimum point, as illustrated in Fig. 7(b). As the operation point is shifted into the overall cavity rollover, the pulse energy increases and the pulse duration decreases, maximizing the achieved peak power. Additionally, the SESAM saturation increases, reducing the effective SESAM losses and thermal lensing.

4. Design guidelines for >100-W, 200-fs Yb:LuO SESAM-modelocked TDLs

We now illustrate an example of how the cavity design and the SESAM parameters can be adjusted to achieve the targeted 200-fs pulse durations at >10 μJ output pulse energies, and consequently output peak powers >20 MW. This pulse duration, τ_p = 200 fs, corresponds to a spectral bandwidth that amounts to ≈45% of the FWHM emission bandwidth of Yb:LuO. For this pulse duration, the effect of the finite gain bandwidth is already significant, as shown in Fig. 5. The targeted intracavity pulse energy is chosen to reflect our criterion for the maximum allowed peak intensity on intracavity optics discussed in section 2.1: for a maximum peak intensity of 150 GW/cm^2 on a spot with a minimum radius of 500 μm, the peak power is limited to ≈590 MW and the corresponding intracavity pulse energy to ≈130 μJ. We therefore consider a laser cavity with a target modelocking point at 120 μJ (intracavity), 200 fs with a repetition rate of 10 MHz, leading to an intracavity average power of 1.2 kW. Note that these limits could be relaxed if our damage-threshold estimate is found to be overly conservative, or if a different stable cavity design with larger modes is found. Therefore, these limits are useful for developing a design target in this paper, but substantially higher intracavity peak powers may ultimately be possible.

Given the available intracavity power and a targeted output power >100 W, we can immediately specify an output coupling rate. We choose this to be 12.5%, yielding 150 W output power. In order to maintain reasonable laser efficiency, the inversion level should not

Optics EXPRESS

be too high, and so we target a design having <20% inversion level, as in our experiments. Consequently, additional passes of the laser on the disk are needed, in order to have enough gain to support the higher OC rate. The number of passes is therefore set to $n_{passes} = 32$.

Another effect of the higher OC rate is a larger difference in gain between cw and pulsed operation compared to Fig. 5. However, simply choosing the SESAM fit parameter ΔR equal to this difference is not enough, for two reasons: (1) The available modulation depth will be reduced due to TPA. (2) Because we target short pulses, there is a pronounced influence of the gain bandwidth on the net cavity rollover, as in Fig. 6(b); to counter-act this effect, and operate close to the net cavity rollover, we need to operate at pulse energies substantially below the SESAM rollover point $E_{p,0}^{SESAM}$. In this way, the effects of increasing SESAM reflectivity and decreasing gain (with respect to pulse energy in the soliton modelocked laser) can balance each other and support stable operation.

To illustrate these points, we show in Fig. 8 the trends for the net cavity gain curve when the SESAM and cavity design parameters are varied. As a starting point for the design procedure, we choose a similar cavity design and the same SESAM as in our high peak-power modelocking experiments presented in section 2 (see Table 1). We then seek to optimize the modelocked operation point according to our criterion $E_{p,max} \approx 2\ E_{p,0}^{cav}$. The varied and constant parameters for each plot are listed in Table 2.

The initial net cavity gain curve is shown in Fig. 8(a) (blue curve). In Fig. 8(a), we show the influence of increasing ΔR. We observe that the cavity rollover occurs below 30 µJ of intracavity pulse energy and there is no net gain for pulsed operation at the desired operation point. With an increased SESAM modulation depth and reduced OC rate, the net cavity gain at the desired operation point increases and exceeds the minimum required to favor pulsed operation over cw operation. At the same time the cavity rollover is shifted to higher pulse energies, shifting the stable modelocked operation region towards the desired operation point. Note that the OC transmission is adjusted in Fig. 8(a) to keep the inversion level constant while increasing ΔR. However, it is not desirable to only increase the modulation depth until the operation point is well within the stable modelocking region, since this would lead to a high laser threshold. Moreover, a higher modulation depth is achieved by increasing the number of quantum wells in the SESAM structure, which also results in increased SESAM losses.

Therefore, we next set the modulation depth to 10% (and the OC rate to 12.5%) and seek to shift the stability region to higher pulse energies by varying the laser mode radius on the SESAM, as shown in Fig. 8(b). As the laser mode size on the SESAM increases, TPA is reduced and the stability region shifts to higher pulse energies. However, the SESAM is also less saturated and this leads to an overall reduction of the SESAM reflectivity, with consequences on the net cavity gain. This also introduces higher losses, since the SESAM is not operated at the maximum of its reflectivity curve. As can be seen from Fig. 8(b), for laser mode radii >2.6 mm, the operation point is well within the stable modelocking region: we subsequently set the mode radius to 2.6 mm. In this configuration, the operation point is already within the stable modelocking region.

For completeness, we also consider the effect of the other SESAM parameters: saturation fluence F_{sat} and rollover fluence F_2. As illustrated in Fig. 8(c), for increasing saturation fluences, the stable modelocking region is slightly shifted to higher pulse energies. However, the quantum wells being less saturated, the overall net cavity gain decreases and the SESAM losses increase. For our targeted operation point, a saturation fluence of 120 µJ/cm^2 is best suited.

Finally, we study the influence of the F_2 parameter on the cavity net gain curve: as shown in Fig. 8(d), this parameter has very little influence on the cavity net gain, as the finite gain bandwidth is the main limiting effect for the targeted pulse parameters.

Optics EXPRESS

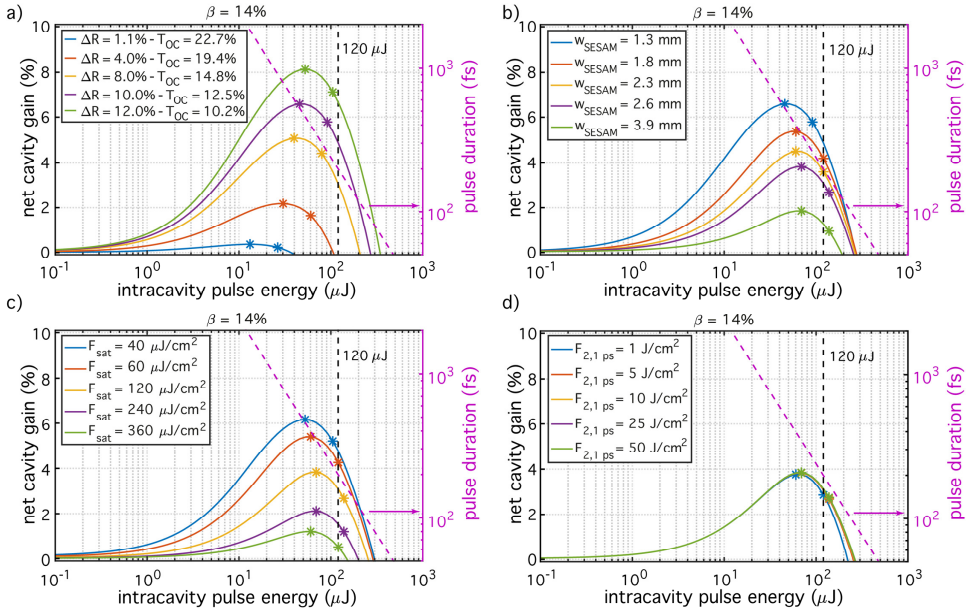

Fig. 8. Net cavity gain as a function of intracavity pulse energy and optimization of the cavity and SESAM parameters for stable modelocking at 120 µJ and 200 fs. Black dashed line: desired intracavity pulse energy, purple line: soliton pulse duration. a) Variation of the SESAM modulation depth. The OC transmission is adjusted to keep the total losses constant. b) Scaling of the laser mode radius on the SESAM. c) Scaling of the SESAM saturation fluence. d) Scaling of the SESAM reference F_2 coefficient for a pulse duration of 1 ps. The stable modelocking region is indicated by the two markers on each curve.

Table 2. Constant and varied parameters used in each step of the modelocking optimization procedure. In bold: adapted parameters in each step.

	SESAM parameters				Cavity design		OC
	F_{sat}	ΔR	ΔR_{ns}	$F_{2,\,1\,ps}$	w_{SESAM}	n_{passes}	T_{OC}
Initial	120 µJ/cm²	1.1%	0.05%	5 J/cm²	1.3 mm	32	22.7%
Fig. 8(a)[a]	120 µJ/cm²	**1.1 – 12.0%**	**0.05 – 0.60%**	5 J/cm²	1.3 mm	32	**22.7 – 10.2%**
Fig. 8(b)	120 µJ/cm²	10.0%	0.50%	5 J/cm²	**1.3 – 3.9 mm**	32	12.5%
Fig. 8(c)	**40 – 360 µJ/cm²**	10.0%	0.50%	5 J/cm²	2.6 mm	32	12.5%
Fig. 8(d)	120 µJ/cm²	10.0%	0.50%	**1 – 10 J/cm²**	2.6 mm	32	12.5%

[a]In the first step [Fig. 8(a)], the modulation depth ΔR is the parameter of interest. Since the modulation depth and the nonsaturable losses are both determined by the number of QWs of the SESAM structure, ΔR_{ns} is varied accordingly (5% of ΔR). Additionally, in order to keep the inversion level constant, the OC transmission is also changed.

The optimized laser configuration is summarized in Table 3. With an OC transmission of 12.5%, this configuration corresponds to an output peak power of 66 MW. Concerning further power scaling, note that for a given cavity design, the achievable output peak power is constrained by the tolerable intracavity peak power. However, our maximum intensity constraint was already conservative for operating at 600 fs, and the damage threshold will increase for 200-fs pulses [50]. If the peak power constraint can be relaxed by a factor of 4 via optimized optics and cavity design, then the number of passes on the disk, OC rate, and SESAM modulation depth ΔR can all be reduced by a corresponding factor for the same output power. This alternative configuration would significantly simplify the SESAM and cavity design.

Optics EXPRESS

Table 3. Summary of the cavity and SESAM parameters optimization for stable modelocked operation at an intracavity pulse energy of 120 µJ and a pulse duration of 200 fs, with an OC transmission of 12.5% and 32 passes through the thin disk.

	SESAM parameters				Cavity design		OC	Expected output performance			
	F_{sat}	ΔR	ΔR_{ns}	$F_{2,\,1\,ps}$	w_{SESAM}	n_{passes}	T_{OC}	P_{avg}	τ_p	E_p	P_{pk}
Optimized laser configuration	120 µJ/cm^2	10 %	0.50 %	5 J/cm^2	2.6 mm	32	12.5 %	150 W	200 fs	15 µJ	66 MW

The presented optimized laser configuration allowing for high peak-power modelocking at short pulse durations require adjusting both the SESAM parameters and the cavity design. These requirements have consequences on the SESAM design, surface flatness and thermal properties. Operating with large spot sizes on the SESAM (w_{SESAM} >1.2 mm) calls for large-area SESAMs with a high surface flatness and low thermal lensing in order to avoid modal instabilities. Moreover, the required large saturation fluence and modulation depth can be achieved by increasing of the number of QWs of the SESAM structure, which requires additional strain-compensating layers in order to keep the crucial high surface quality. Recently, we have successfully grown high-quality SESAMs with a large number of QWs [51] and investigated a novel direct bonding technique resulting in superior SESAM flatness and thermal properties [52]. These newly developed technologies enable SESAM structures fulfilling the requirements for high peak-power, short-pulsed modelocked operation.

5. Conclusion and outlook

We demonstrated the first peak power scaling of a SESAM-modelocked Yb:LuO TDL to more than 10 MW. Our cavity design based on an 8-pass geometry allowed us to operate at comparatively low intracavity powers and scale the peak power by increasing the cavity length. We achieved high peak-power modelocking at output powers up to 90 W. The highest peak-power was obtained at 82 W with 616-fs pulses at a repetition rate of 9.5 MHz. The corresponding pulse energy of 8.6 µJ and peak power of 12.3 MW are the highest demonstrated to date with a TDL based on Yb:LuO. These results were achieved thanks to the high quality of our very thin 110-µm-thick Yb:LuO disk contacted on diamond, which resulted in negligible thermal lensing. This allowed us to increase the length of our laser resonator and operate it in a pressure-controlled environment. Due to the low residual nonlinearity of our cavity, intracavity peak powers up to 185 MW were reached.

The presented peak-power-scaling experiments were limited by the onset of instabilities, similar to the limits observed for many years in high-power SESAM-modelocking of TDLs. Therefore, we discussed the challenges of peak power scaling SESAM-modelocked TDLs towards the 100-W, 10-µJ, 200-fs regime. We identified the two main limiting effects as the SESAM reflectivity rollover and the finite gain bandwidth. These effects can jointly be taken into account by calculating an overall net cavity gain for pulsed operation as a function of the intracavity pulse energy in a given laser configuration. Stable modelocked operation can be achieved at intracavity pulse energies exceeding the maximum of this net cavity gain curve $E_{p,0}^{cav}$ up to a factor of ≈2. For short pulse durations where the effect of the gain bandwidth is significant, this optimal operation range does not coincide with the maximum of the SESAM reflectivity, thus requiring a trade-off between robustness to modelocking instabilities and thermal load on the SESAM. In the case of Yb:LuO, we illustrated how the SESAM parameters and the cavity design can be optimized to allow for stable modelocking at high output pulse energies (15 µJ) and short pulse durations (200 fs) by:

- increasing the number of laser passes (≈32) through the thin-disk to allow for higher output coupler transmissions and relaxed intracavity conditions

Optics EXPRESS

- keeping the saturation fluence moderately high (≈120 μJ/cm^2) to allow for high pulse energies with enough saturation of the quantum wells

- increasing the SESAM modulation depth to several percent (≈10%) to overcome the gain reduction at short pulse durations

- increasing the laser mode radius (≈2.6 mm) on the SESAM to operate on the rising edge of the SESAM reflectivity curve

These last two point can be stated more generally: the rate of change in saturable loss with respect to the energy of the soliton must balance the reduced gain due to the finite bandwidth of the gain medium. We expect that this criterion will be applicable both to SESAM modelocked TDLs but also other laser configurations, e.g. KLM TDLs or those incorporating both a Kerr lens and a SESAM.

The required SESAM parameters can be achieved by growing strain-compensated structures with a large number of quantum wells (>8) and carefully designing dielectric top-coatings to tailor the saturation fluence and modulation depth. The enhanced thermal management required by the high SESAM losses due to operation away from the rollover point and the increased cavity mode sensitivity to thermal lensing due to the large spot size can both be addressed by contacting the SESAM using a novel direct substrate transfer technique providing superior flatness and heat removal capabilities.

The ongoing improvements of the SESAM structures combined to the new insights on optimizing modelocked operation at short pulse durations are opening a route to demonstrating SESAM-modelocked Yb:LuO thin-disk oscillators reaching multi-10-MW output peak powers at pulse durations around 200 fs. Additionally, combining the SESAM with other types of loss modulators and achieving a broad gain profile could be key to further scale the output peak of short pulsed TDLs toward >100 MW.

Funding

Swiss National Science Foundation (200020_172644); “The Hamburg Centre for Ultrafast Imaging – Structure, Dynamics and Control of Matter at the Atomic Scale” of the Deutsche Forschungsgemeinschaft (EXC 1074) and the German Ministry of Education and Research (BMBF) (13N14192).

Acknowledgments

The ETH Zurich authors also acknowledge support of the technology and cleanroom facility FIRST of ETH Zurich for advanced micro- and nanotechnology.